

NUMERICAL STUDY OF TWO-PHASE VISCOELASTIC FLOW IN A TWO-DIMENSIONAL T-JUNCTION

Helder M. Matos

Paulo P. Oliveira

heldermiguelmm@hotmail.com

pjpo@ubi.pt

Unidade de Materiais Têxteis e Papeleiros, Departamento de Engenharia Electromecânica,
Universidade da Beira Interior.

Rua Marques D'Avila e Bolama, 6200-001 Covilhã, Portugal

Abstract. *The present investigation is mainly concerned with the construction of a new predictive code for the simulation of two-phase flows when one of the phases may have non-Newtonian, viscoelastic properties. Of the two fundamental approaches to model two-phase flows, we follow the Eulerian one, with both phases treated as interpenetrating continua. Simulations are performed for a steady-state laminar incompressible flow, in a planar 2D bifurcation where the branch makes an angle of 90 degrees with the main arm, and with the continuous phase being a viscoelastic liquid while the dispersed phase is either composed by particles or is a Newtonian fluid. The choice of this geometry is motivated by future application to hemodynamic flows, since it is well-known that vascular diseases tend to occur near the branches of arterial bifurcations. Two-phase flows in bifurcations involving viscoelastic fluids are encountered in other important applications, like the petroleum industries where the bifurcations are used to separate the oil from the natural gas in sub-sea pipelines before being transported to their destination.*

Keywords: *Two-phase flow, Viscoelastic fluid, Bifurcation, Recirculations.*

1. INTRODUCTION

The present investigation is mainly concerned with the construction of a new predictive code for the simulation of two-phase flows when one of the phases may have non-Newtonian, viscoelastic properties. In this communication, the basic equations and the numerical method are outlined, and only preliminary results presented. Of the two fundamental approaches to model two-phase flows (Crowe et al., 1998), we follow the Eulerian one, with both phases treated as interpenetrating continua (Oliveira and Issa, 2003). Simulations are performed for a steady-state laminar incompressible flow, in a planar 2D bifurcation where the branch makes an angle of 90 degrees with the main arm, and with the continuous phase being a viscoelastic liquid while the dispersed phase is either composed by particles or is a Newtonian fluid. One work addressing the simultaneous simulation of the flow of Newtonian and viscoelastic fluids was by Dheur and Crochet (1989) but it only considered stratified flows in which the two phases are separated.

The results obtained with the new algorithm will be compared with the results obtained for single-phase viscoelastic flow through a T-junction under the same conditions. The choice of this geometry is motivated by future application to hemodynamic flows, since it is well-known that vascular diseases tend to occur near side branches of arterial bifurcations (Ku, 1997 and Salzar et al., 1995). Another important application of bifurcations is in the petroleum industries which are used to separate the oil from the natural gas in the subsea pipelines before being transported to their destination (Baker et al., 2007). In the next paragraphs we discuss briefly these two types of applications.

In the human circulatory system, blood drains along successive bifurcations of arteries producing a very high complex flow. The most common manifestation of arterial disease is atherosclerosis. One of the principal areas of research investigating the cause of atherosclerosis is the role of blood flow and its interaction with the artery wall through the action of fluid shear stress. Complex flow in bifurcations promotes the appearance of regions of flow separation and recirculation, where wall shear stresses are very low, thus promoting the possibility of adhesion of platelets, red cells and lipoids, which ultimately result in the formation of atherosclerotic plaques and thrombi (Liepsch et al., 1982). The arteries where the atherosclerotic plaques grow, lose their elasticity and become narrower. Besides, with time the arteries accumulate deposits of calcium and become fragile and break up (Ku, 1997). This mechanism has been established by many studies, e.g. Caro et al. (1971), Zarins et al. (1983), and Ku et al. (1985). At the same time in other zones high wall shear stresses are encountered, where the endothelium of the arteries may be damaged, (Fry, 1969 and Joris et al., 1982), leading to a decrease of artery-wall relaxation and to atherosclerotic disease. In zones with high shear stress there also occurs hemolysis, with the degradation of the red cells and undesirable release of hemoglobin in the blood stream (Liepsch et al., 1982).

In this area of research the majority of works in the literature use a single-phase computational fluid dynamics model, however blood is a complex fluid that consists in a suspension of multiple constituents like platelets, leucocytes and erythrocytes in plasma (Anand et al., 2004). The interaction between blood constituents during the flow endows it with viscoelastic properties. Thus blood exhibits shear-thinning in viscosity, is thixotropic and viscoelastic (e.g. Miranda et al., 2008). The changes in viscosity are associated with the energy dissipated during flow primarily due to friction and deformation of red blood cells and red blood cell aggregation, while the energy stored during flow due to orientation and deformation of red blood cells promotes changes in the blood elasticity (Owens, 2006 and Leuprecht et al., 2001). In a recent hemodynamic simulation, Jung et al. (2006) used a multiphase theory to represent the blood; however the viscoelasticity effects were neglected and blood was assumed as a non-Newtonian inelastic fluid with shear-thinning viscosity.

According to Long et al. (2005) only for shear rates higher than 500 s^{-1} , typically occurring in the larger arteries, can blood present a Newtonian behaviour.

In engineering applications, bifurcations are commonly used in liquid distribution systems; however when a two-phase fluid flows through a T junction the phase distribution between the main and branch ducts are inevitably different, affecting the flow control and processing facilities downstream. In some situations, like in the petroleum industries, this phenomenon is advantageous and used for the first stage of oil and gas phase separation, with attending improvement in the efficiency of the transport system (Margaris, 2007) and reduction of the processing load of the main separator which are usually very large, and much more complex and expensive than a simple T-junction. There are many works in this research area, in order to predict the phase separation in two-phase flows through T-junctions like Issa and Oliveira (1994), Hatziaavramidis et al. (1997), or Wang et al. (2008). Many configurations for the orientation of the branch duct (upward, downward, etc.), diameters of the ducts, inlet flow patterns, and so on, were assumed in order to increase the separator efficiency. However in those works the possible viscoelastic characteristics of the liquids were not taken into consideration.

We follow the finite-volume method in non-orthogonal coordinates, employing non-staggered meshes in which all variables are stored at the centre of cells forming the mesh (Oliveira, 1992). For non-Newtonian fluids, rheological equations of state will be needed and we intend to obtain the stress tensor from finite-extensibility constitutive models, like the FENE-CR (Chilcot and Rallison, 1988) or the FENE-P (Bird et al., 1987). The coupling between velocity and stress fields is affected with the method of Oliveira et al. (1998; 1999). In addition, and with view to maintain good level of accuracy, the convective terms in the governing equations are represented by the high-resolution scheme CUBISTA of Alves et al. (2003). Preliminary results of single-phase simulations are provided by Matos et al. (2007a, 2007b and 2007c), which will be useful for future comparisons against results from the multiphase theory.

2. DIFFERENTIAL EQUATIONS

For an incompressible and isothermal two-phase flow the equations that need to be solved (Crowe et al., 1998; Oliveira and Issa 2003) are the conservation of mass for phase k (c for continuous and d for dispersed):

$$\frac{\partial}{\partial t} \alpha_k + \nabla \cdot (\alpha_k \mathbf{u}_k) = 0 \quad (1)$$

and the conservation of momentum:

$$\frac{\partial}{\partial t} (\rho_k \alpha_k \mathbf{u}_k) + \nabla \cdot (\rho_k \alpha_k \mathbf{u}_k \mathbf{u}_k) = \nabla \cdot (\alpha_k \mathbf{T}_k) + \rho_k \alpha_k \mathbf{g} + \mathbf{M}_k \quad (2)$$

In addition, the condition of phase compatibility implies that the sum of the two volume fractions should be equal to unity:

$$\alpha_c + \alpha_d = 1 \quad (3)$$

In these equations, α is the volume fraction, \mathbf{u} is the phase average velocity, ρ is the density, assumed constant for both phases, g is the acceleration of gravity, \mathbf{T} is the total stress tensor that will be split into an isotropic pressure and a deformation stress ($\boldsymbol{\tau}$) as:

$$\mathbf{T}_k = -p_k \boldsymbol{\delta} + \boldsymbol{\tau}_k \quad (4)$$

Substituting the stress \mathbf{T}_k from Eq. (4) into Eq. (2) we obtain:

$$\frac{\partial}{\partial t}(\rho_k \alpha_k \mathbf{u}_k) + \nabla \cdot (\rho_k \alpha_k \mathbf{u}_k \mathbf{u}_k) = -\alpha_k \nabla p_k - p_k \nabla \alpha_k + \alpha_k \nabla \cdot \boldsymbol{\tau}_k + \boldsymbol{\tau}_k \cdot \nabla \alpha_k + \rho_k \alpha_k \mathbf{g} + \mathbf{M}_k \quad (5)$$

In equations (2) and (5) the interface momentum transfer term denoted by \mathbf{M}_k is composed by drag (\mathbf{M}_k^D), virtual mass (\mathbf{M}_k^{VM}), and an interface-average stress (\mathbf{M}_k^I). The most important component in the fluid-particle interaction is the drag force, generated by the resistance to relative motion in a viscous flow and the virtual mass which results from relative phase acceleration. Those components of the interface momentum transfer term are given by:

$$\mathbf{M}_k^D = C_f \left[\alpha_k \hat{\alpha}_k (\hat{\mathbf{u}}_k - \mathbf{u}_k) - \eta_k \nabla \alpha_k \right] \quad (6)$$

$$\mathbf{M}_k^{VM} = \rho_c C_{VM} \alpha_k \hat{\alpha}_k \left(\frac{D\hat{\mathbf{u}}_k}{Dt} - \frac{D\mathbf{u}_k}{Dt} \right) \quad (7)$$

$$\mathbf{M}_k^I = \int_{A_i} \mathbf{T}_{ki} \cdot \mathbf{n}_k da = -\mathbf{T}_{ki} \cdot \nabla \alpha_k = p_{ki} \nabla \alpha_k - \boldsymbol{\tau}_{ki} \cdot \nabla \alpha_k \quad (8)$$

In equations (6) to (8) the symbol ($\hat{\cdot}$) denotes the other phase and the index (i) refers to interface conditions. In equation 6 related to the drag term, the coefficient C_f is expressed by:

$$C_f = \frac{3}{4} \frac{C_D u_r}{d_p} \quad (9)$$

where u_r is the relative velocity ($u_r = |\mathbf{u}_d - \mathbf{u}_c|$), d_p is the particle diameter and the drag force coefficient C_D is obtained assuming the standard curve for drag around a sphere (Crowe et al., 1998) and expressed for:

$$C_D = \frac{24}{\text{Re}} \left[1 + 0.15 \text{Re}_p^{0.687} \right] \quad (10)$$

The Reynolds number ($\text{Re} = \rho_c u_r d_p / \mu_c$) is defined with the continuous phase viscosity and the relative velocity.

After inserting the auxiliary relationships expressed Eqs. (6)-(8) into Eq. (5), and dividing the resulting equation by α_k , we arrive at the momentum equation in a non-conservative

form, where the material derivative $D(\cdot)/Dt = \partial(\cdot)/\partial t + \mathbf{u} \cdot \nabla(\cdot)$ represents the local variation of a property following a fluid element, thus:

$$\begin{aligned} \rho_k \frac{D\mathbf{u}_k}{Dt} = & -\nabla p_k - p_k \frac{\nabla \alpha_k}{\alpha_k} + \nabla \cdot \boldsymbol{\tau}_k + \boldsymbol{\tau}_k \cdot \frac{\nabla \alpha_k}{\alpha_k} + \rho_k \mathbf{g} \\ & + C_f \left[\hat{\alpha}_k (\hat{\mathbf{u}}_k - \mathbf{u}_k) - \eta_k \frac{\nabla \alpha_k}{\alpha_k} \right] + \rho_c C_{VM} \hat{\alpha}_k \left(\frac{D\hat{\mathbf{u}}_k}{Dt} - \frac{D\mathbf{u}_k}{Dt} \right) + p_{ki} \frac{\nabla \alpha_k}{\alpha_k} - \tau_{ki} \frac{\nabla \alpha_k}{\alpha_k} \end{aligned} \quad (11)$$

If we assume that $\tau_{ki} = \tau_k$ and define a dispersion coefficient \mathcal{S}_k as $\mathcal{S}_k = -(p_{ki} - p_k) + C_f \eta_k$, then the final form of the momentum equation is given by:

$$\rho_k \frac{D\mathbf{u}_k}{Dt} = -\nabla p_k + \nabla \cdot \boldsymbol{\tau}_k + \rho_k \mathbf{g} - \mathcal{S}_k \frac{\nabla \alpha_k}{\alpha_k} + \hat{\alpha}_k C_f (\hat{\mathbf{u}}_k - \mathbf{u}_k) + \rho_c C_{VM} \hat{\alpha}_k \left(\frac{D\hat{\mathbf{u}}_k}{Dt} - \frac{D\mathbf{u}_k}{Dt} \right) \quad (12)$$

When the possibility of having a viscoelastic fluid in a two-phase flow arises, we need a new equation to express the stress tensor evolution, likewise to turbulent flows, where an expression is needed for the Reynolds stress tensor. In both cases, empirical relationships are used, based on the best fit with the physical problem at hand.

For a homogeneous polymeric solution the continuous-phase stress tensor $\boldsymbol{\tau}_c$ can be written as the sum of a Newtonian solvent and a polymeric contribution $\boldsymbol{\tau}_c = \boldsymbol{\tau}_s + \boldsymbol{\tau}_p$ (Bird et al., 1987). This solvent contribution is expressed by a Newtonian law for viscosity.

$$\boldsymbol{\tau}_s = \eta_s (\nabla \mathbf{u} + \nabla \mathbf{u}^T) \equiv 2\eta_s \mathbf{D} \quad (13)$$

In equation (13), the superscript "T" designates the transpose of a tensor, \mathbf{D} is the rate of strain tensor and η_s is the solvent viscosity, while the total viscosity is given by the sum of solvent and polymeric viscosities ($\eta_0 = \eta_s + \eta_p$). When a polymeric solution is assumed we have to define another parameter which relates the solvent and polymer viscosities, and a possibility is through the retardation ratio $\beta \equiv \eta_s / \eta_0$, or equivalently through a concentration parameter $c \equiv \eta_p / \eta_s$, where the two are related by $\beta \equiv 1/(1+c)$.

The viscoelastic contribution is expressed by a rheological constitutive model (Bird et al., 1987), derived from finite extensibility non-linear dumbbells (FENE, Finite Non-linear Extensible Elastic). We have here used the FENE-CR model proposed by Chilcott et al. (1988), where the stress tensor is expressed by:

$$\boldsymbol{\tau} + \lambda \left(\overset{\nabla}{\frac{\boldsymbol{\tau}}{f(\boldsymbol{\tau})}} \right) = 2\eta_p \mathbf{D} \quad (14)$$

where λ is the relaxation time of the fluid. The symbol $\overset{\nabla}{\cdot}$ denotes Oldroyd's upper convected derivative,

$$\overset{\nabla}{\boldsymbol{\tau}} = \frac{D\boldsymbol{\tau}}{Dt} - [\nabla \mathbf{u}^T \cdot \boldsymbol{\tau} + \boldsymbol{\tau} \cdot \nabla \mathbf{u}] \quad (15)$$

and the function $f(\boldsymbol{\tau})$ is given by:

$$f(\boldsymbol{\tau}) = \frac{L^2 + (\lambda / \eta_p) \text{tr}(\boldsymbol{\tau})}{L^2 - 3} \quad (16)$$

where L^2 is the extensibility parameter, here assumed as constant ($L^2 = 100$), and tr represents the trace operator.

3. DISCRETISATION AND SOLUTION PROCEDURE

The numerical method solves the full three-dimensional, two-fluid model transport equations (composed by six momentum and two continuity equations), whereby both phases are treated as interpenetrating dispersed continua in an Eulerian frame (Issa and Oliveira, 1994). The use of an Eulerian approach is highly recommended for two-phase flows when the void fractions of the two fluid phases are comparable, like what can occur in the cases here considered

The differential equations described before are discretized using the finite-volume method: they are integrated in space over the control-volumes forming the computational mesh, thus leading to a set of linearized algebraic equations where the unknowns are the nodal values of the several variables (Patankar, 1980 and Ferziger and Peric, 1996). In general, these algebraic equations have the following form:

$$a_P \phi_P = \sum_F a_F \phi_F + S_\phi \quad (17)$$

where a_F and a_P are coefficients accounting for convection and diffusion influences, from any surrounding cell F (6 in a general 3D problem 4 in 2D) onto the cell P in question, and S are source terms containing all other influences. The discretized momentum equation for both phases (at cell P), with implicit treatment for drag and virtual mass is:

$$\begin{aligned} a_P \mathbf{u}_P = & \sum_F a_F \mathbf{u}_F - B_P [\Delta p]_P - V_P \mathcal{A}_P \frac{[\nabla \alpha]_P}{\alpha_P} + \hat{\alpha}_P C_f \hat{\mathbf{u}}_P V_P \\ & + \left(\frac{\rho' V}{\delta t} \right)_P \mathbf{u}_P^0 + S_u' + \rho_c \hat{\alpha}_P C_{VM} \sum_F \hat{\alpha}_F^c (\hat{\mathbf{u}}_P - \hat{\mathbf{u}}_F) + S_u^{HOS} \end{aligned} \quad (18)$$

And the central coefficient of the momentum equation is given by:

$$a_P = \sum_F a_F + \left(\frac{\rho' V}{\delta t} \right)_P + \hat{\alpha}_P C_f V_P \quad (19)$$

In the above equations which are valid for both phases but where the phase index was omitted for a question of simplicity, V_P is the cell volume, B_P are the cell surface areas, $[\Delta p]_P$ and $[\Delta \alpha]_P$ are pressure and void fraction differences evaluated at the cell centre P , $\overline{\alpha}_P$ is an average value of the volume fraction over the cell P , calculated as $\overline{\alpha}_P = \sum_f \alpha_f$ in

order to prevent problematic situations of overflow when $\alpha_f \rightarrow 0$, where α_f represents linearly interpolated cell face values, ρ' is an effective density corrected for virtual mass effects as $\rho' \equiv \rho(1 + \hat{\alpha} C_{VM} \rho_c / \rho)$, S_u' is the source term containing all contributions not explicitly written, such the buoyancy term, and S_u^{HOS} is the source term related to the implementation of a high-resolution scheme CUBISTA developed by Alves et al. (2003). Each neighbour coefficient a_F is composed by diffusion and virtual-mass-corrected convection contributions ($a_F = a_F^{\mathcal{D}} + a_F^{\mathcal{C}}$).

For the rheological constitutive equation here considered, the FENE-CR model, we can rewrite Eq. (14) including the relationship from Eq. (15), as:

$$\boldsymbol{\tau} + \lambda \frac{D}{Dt} \left(\frac{\boldsymbol{\tau}}{f(\boldsymbol{\tau})} \right) = 2\eta_p \mathbf{D} + \frac{\lambda}{f(\boldsymbol{\tau})} [\nabla \mathbf{u}^T \cdot \boldsymbol{\tau} + \boldsymbol{\tau} \cdot \nabla \mathbf{u}] \quad (20)$$

And the discretized constitutive equation is given by:

$$a_p^\tau \boldsymbol{\tau}_p = \sum_F a_F^\tau \boldsymbol{\tau}_F + \frac{\lambda}{f(\boldsymbol{\tau})} \frac{\boldsymbol{\tau}_p}{\delta t} + S_\tau [\nabla \mathbf{u}] + S_\tau^{HOS} \quad (21)$$

where the central coefficient of the constitutive FENE-CR model is:

$$a_p^\tau = \sum_F a_F^\tau + \frac{\lambda}{f(\boldsymbol{\tau})} \frac{V_p}{\delta t} + V_p \quad (22)$$

The volume fractions are obtained from solution of one of the continuity equations, typically that for the dispersed phase which is discretized and solved as a transport equation for $\alpha \equiv \alpha_d$, and the other phase volume fraction is the obtained from $\alpha_c = 1 - \alpha_d$ (Eq. (3)). This and other forms to obtain the volume fraction are discussed in Oliveira and Issa (2003).

The methodology employs a non-staggered mesh (e.g. Oliveira, 1992) in witch all variables are stored at the centres of each cell in the mesh. In order to ensure an adequate coupling between the velocity and pressure fields in this type of meshes, we follow the interpolation technique of Rhie and Chow (1983) to evaluate the velocity components and obtain the convective fluxes at the cell faces. The precise form is given in Oliveira (1992) as

$$\overline{a_p} \tilde{\mathbf{u}}_f = \sum_F \overline{a_F} \mathbf{u}_F - B_f [\Delta p]_f - V_p \overline{\mathcal{A}_p} \frac{[\Delta \alpha]_f}{(\overline{\alpha_p})_f} + \overline{\hat{\alpha}_f} \tilde{\mathbf{u}}_f V_f + \left(\frac{\rho' V}{\delta t} \right)_f \tilde{\mathbf{u}}_f^0 + S_u' \quad (23)$$

where the overbar means arithmetic averaging and the symbol (\sim) means variables obtained through a special interpolation technique akin to that of Rhie and Chow (1983). The gradient of α is obtained directly at the cell face f and not by averaging: $[\Delta \alpha]_f = \alpha_F - \alpha_P$.

The coupling between the stress and the velocity fields is obtained using a procedure similar to that of Oliveira et al. (1998), which was later subjected to improvements (Oliveira and Pinho, 1999), and in the most recent form, following the work of Matos et al. (2007b), which was aimed at obtaining solutions independent of the time step value used. The expression used to obtain the stresses at the cell faces is given by:

$$\begin{aligned}
(\tilde{\tau}_{ij}) = (\overline{\tau}_{ij})_f + \frac{1}{(1 + a_0^\tau / V_p)} & \left[-\frac{1}{V_p} \left(\eta_p B_{fi} [\Delta u_j]_f + \eta_p B_{fj} [\Delta u_i]_f - \frac{2}{3} \eta_p \sum_k B_{fk} [\Delta u_k]_f \delta_{ij} \right) \right. \\
& \left. + \frac{1}{V_f} \left(\eta_p B_{fi} [\Delta u_j]_f + \eta_p B_{fj} [\Delta u_i]_f - \frac{2}{3} \eta_p \sum_k B_{fk} [\Delta u_k]_f \delta_{ij} \right) \right]
\end{aligned} \quad (24)$$

In these equations B_{fi} is the i -component of the cell face area aligned with direction f , V_p and V_f are the volumes of the cell centred in P and in the face f . The superscript (\sim) is used to denote a special type of interpolation (Oliveira et al., 1998), while the superscript $(-)$ corresponds to linear interpolations.

In the present work we employ orthogonal meshes, however the method can apply non-orthogonal meshes (Oliveira, 1992), which require a transformation from the orthogonal coordinate system (x_1, x_2, x_3) onto a general non-orthogonal coordinate system (ξ_1, ξ_2, ξ_3) following the procedure explained in Oliveira et al. (1998). This transformation has the advantage of working with the equations written in a strong conservation form, which helps to obtain conservativeness in the final discretized equations.

All the equation sets resulting from discretization of the velocity and pressure differential equations are linearized and solved sequentially with an iterative procedure. The algorithm used is prepared for the unsteady-state calculations; however, it can also be used for steady state calculations, where the iterations are substituted by a fictitious progress in time, producing an effect similar to the use of a sub-relaxation factor.

The diffusive terms and the gradient pressure term in the governing equations were represented by central differences (CDS, second order), while the convective terms are represented by a high resolution scheme, the CUBISTA scheme developed by Alves et al. (2003). This scheme possesses good accuracy, being of third-order in space for smooth flows, and good characteristics in terms of iterative convergence for viscoelastic flows.

The algorithm used is based on the algorithm SIMPLEC of Van Doormaal and Raithby (1984) which allows coupling of the velocity and pressure fields in order to verify the continuity equation in steady-state flows.

3.1 Solution algorithm

The sets of discretized equations are solved iteratively in a sequential manner following the pseudo time-marching approach here explained, where new or intermediate values are denoted with an asterisk, and values from the previous time step with index n .

- 1- Obtain cell-centered stresses (τ) from the implicit equation

$$a_p^\tau \tau_p^* = \sum_F a_F^\tau \tau_F^* + (S_\tau)^n \quad (25)$$

and store the central coefficient a_p^τ .

- 2- Compute cell face stresses $\tilde{\tau}$ from Eq. (24) based on the newly obtained stresses τ^* of Eq. (25) with central coefficient a_p^τ and velocity gradients evaluated at the previous time step.

- 3- Solve for the continuous phase Cartesian velocity components at cell centres, u_c^* from the discretized momentum conservation Eq. (18) for the continuous phase.

$$a_P^\tau \mathbf{u}_{c,P}^* = \sum_F a_F^\tau \mathbf{u}_{c,F}^* + (S_{u,c})^\tau \quad (26)$$

4- Solve for the dispersed phase Cartesian velocity components at cell centres, \mathbf{u}_d^* from the discretized momentum conservation Eq. (18) for the dispersed phase

5- Obtain cell face velocities from equation 23 and compute the corresponding mass flow rates.

$$F_f^* = \sum_i (\rho B_{fi} \tilde{u}_i^*)_f \quad (27)$$

6- Solve the pressure-correction equations following the SIMPLEC algorithm of Van Doormaal and Raithby (1984) as modified for time-marching by Issa and Oliveira (1994); correct the pressure field, p^* , the velocity field, \mathbf{u}^{**} , and the mass flow rates, F_f^{**} , which will now satisfy the continuity constraints.

7- Solve all additional scalar equations, like the turbulence or temperature equations when these are considered in the problem at hand.

8- Solve implicitly the dispersed phase continuity equation in order to obtain an updated void fraction, to be used to determine upwinded cell-face void fractions $\tilde{\alpha}_f$, which are stored in memory.

9- Check for convergence to a steady state, when the norm of the residuals of all equations has fallen below a prescribed tolerance (10^{-8}). At this point overall continuity for the sum of the continuous and dispersed phases is satisfied, together with individual continuity for the dispersed phase. Therefore continuity will also be satisfied for the continuous phase. Otherwise, take the variables as pertaining to a new time level (n+1) and go back to step 1. In this work a very low tolerance for the residuals is imposed, in order to obtain independent solutions with the time step value here employed for simulations with high values of Deborah number and very low time step values, like those considered in Matos et al. (2007a).

Implicit solution of the linear sets of equations in steps 1, 3, 4 and 6 is carried out by application of standard preconditioned conjugate gradient methods (Oliveira, 1992).

4. GEOMETRY AND COMPUTATIONAL MESH

Simulation were done for conditions similar to those of past works (e.g. Matos et al., 2007a) in the 2D T-shaped geometry of Fig.1, having a constant cross-section area with height H equal to 0.01 m.

The inlet flow is applied in block 1 at $x = -3.5H$, where a parabolic profile of velocity is imposed with an average velocity of $u_1 = 0.0745$ m/s; the outlets are located at $x = 22.5H$ and $y = 20.5H$, where conditions of vanishing axial variation are imposed for all quantities (i.e. $\partial/\partial x = 0$ in the horizontal duct and $\partial/\partial y = 0$ in the vertical duct), except the pressure which is obtained from linear extrapolation from the inside of the channel. These conditions in the outlet were obtained when the flow is supposed to be fully developed and that guarantees that the lengths of the branch and main ducts are sufficiently long.

$$De = \frac{\lambda u_1}{H} \quad (29)$$

The fluid had a density of $\rho = 1150 \text{ kg/m}^3$ and a viscosity of $\eta_0 = 0.0084 \text{ Pa.s}$; in the case of viscoelastic fluids, the ratio between the viscosity of the solvent and the total viscosity of was 0.8, in agreement with results for single-phase theory, giving a solvent viscosity $\eta_s = 0.0067 \text{ Pa.s}$ and a polymeric viscosity $\eta_p = 0.0017 \text{ Pa.s}$.

Due to the complexity of the geometry, the mesh to map the domain had to be constituted by more than one block. In the present work, a mesh with 6 structured blocks (B1-B6) was employed, as represented in the figure 1; this mesh is orthogonal but non-uniform, with increased concentration of cells near the bifurcation zone where the stress gradients are expected to be higher. In order to construct a non-uniform mesh we use a geometrical progression with a constant ratio in both directions (f_x and f_y , given in Table 1), and this progression factors were chosen to be close to unity in order to guarantee a smooth cell-size variation.

In the bifurcation area, two recirculation zones are formed close to the walls, a vertical and a horizontal, and these are characterized by their starting and ending points: a flow separation point, X_s and Y_s for the horizontal and vertical recirculation, and a point of flow recovery X_R e Y_R , where the recirculations terminate. The recirculation lengths, X_L and Y_L , are determined by the difference between their recovery and separation points.

A study of mesh refinement has been carried out by Matos et al. (2007a), using three meshes progressively refined, having 6400, 12800 and 25600 control-volumes, and after applying Richardson's extrapolation technique (Richardson, 1910) to obtain the convergence rate of the numerical method and to evaluate a more accurate solution, it was possible to evaluate the discretization error. From this study it was concluded that the intermediate mesh was sufficient for adequate accuracy of the calculations.

Table 1. Summary of the main characteristics of the computational mesh.

Block	N° of cells $NX \times NY$	Length x [m]	Length y [m]	f_x	f_y
B1	40×40	$-3.5 \rightarrow -0.5$	$-0.5 \rightarrow 0.5$	0.95260	1.00000
B2	40×40	$-0.5 \rightarrow 0.5$	$-0.5 \rightarrow 0.5$	1.00000	1.00000
B3	100×40	$0.5 \rightarrow 12.5$	$-0.5 \rightarrow 0.5$	1.02657	1.00000
B4	40×100	$-0.5 \rightarrow 0.5$	$0.5 \rightarrow 10.5$	1.00000	1.02385
B5	20×40	$12.5 \rightarrow 22.5$	$-0.5 \rightarrow 0.5$	1.06413	1.00000
B6	40×20	$-0.5 \rightarrow 0.5$	$10.5 \rightarrow 20.5$	1.00000	1.06413

5. RESULTS AND CONCLUSIONS

In past works (Matos et al., 2007a, 2007b and 2007c) we have obtained results using single-phase theory for simulations of Newtonian and non-Newtonian viscoelastic flows through a T-junction, where the properties of the fluid were adjusted as to be identical to those of blood since our ultimate goal is to apply the method to hemodynamics. In those works we addressed the influence of elasticity through the variation of the Deborah number and the retardation ratio, with a decrease in the retardation ratio having the same meaning as an increase of the polymer concentration in the fluid. The results obtained will here be presented and discussed in terms of non-dimensional variables, using for length scale the height of the inlet channel (H ; e.g. $Y = y/H$), for velocity scale the average velocity in inlet

flow (u_1) and for the stresses the value of the wall shear stress in the inlet for fully developed steady flow (τ_{w0}).

In the following figures we present results obtained with the single-phase theory, while a comparison against results with the multiphase theory are left for future communications. In figure 2 we show the flow streamlines for a constant retardation ratio $\beta = 0.8$ and different Deborah numbers, $De = 1$ and $De = 2$.

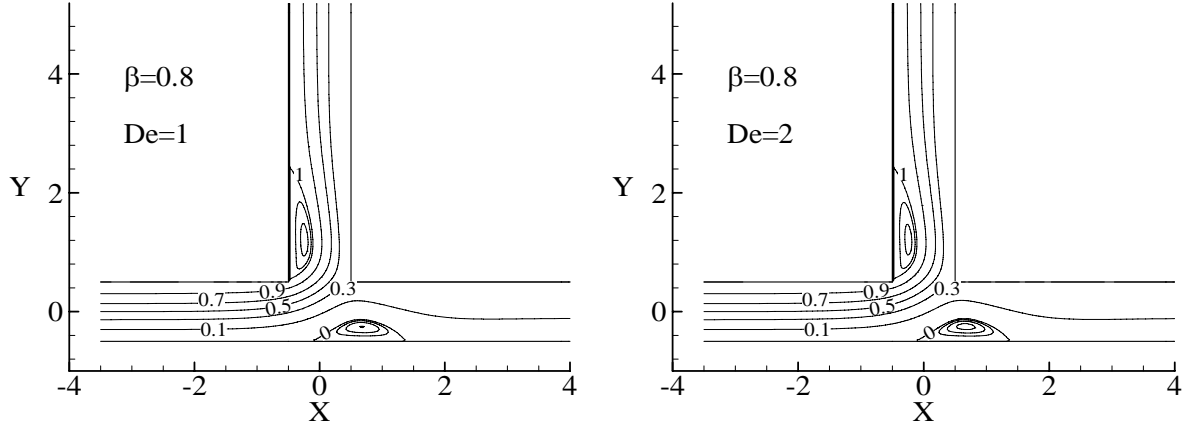


Figure 2- Variation of the flow streamlines for a constant retardation ratio ($\beta = 0.8$) and two Deborah numbers ($De = 1$ and $De = 2$).

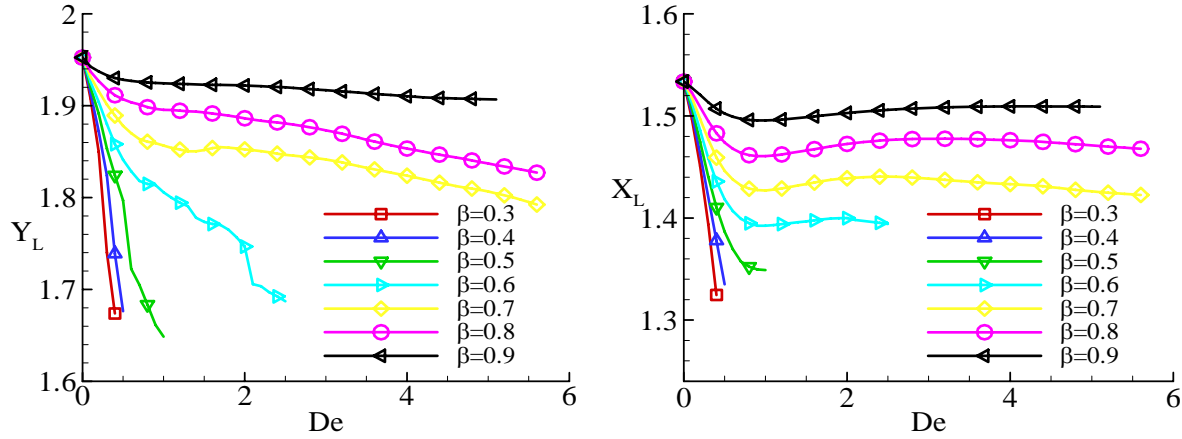


Figure 3- Variation of the vertical and horizontal recirculation lengths with De and β .

From this figure it is possible to observe the two recirculations created in T-junction flows. The recirculation lengths and intensity, stress field and other important flow characteristics change with variation of elasticity, and in the following figures we show an assessment of this for each variable.

Figure 3 shows results relative to the length of recirculations created along the x and y directions, obtained through a profile of velocity along the horizontal ($Y = -0.5$) and vertical ($X = -0.5$) channel walls, with the variation of Deborah number and retardation ratio. From this figure, we note that the increase of elasticity, through the increase of Deborah or decreasing of the retardation ratio results in a decrease in the horizontal and vertical recirculation lengths and this decrease is more pronounced for low values of Deborah number

and retardation ratios. In the horizontal recirculation the variation is almost inexistent for high values of Deborah number and retardation ratio.

Figure 4 shows the variation of the vortex intensity in the branch and the main ducts, as a function of the Deborah number and the retardation ratio. In the vertical duct, a reduction of the vortex strength is observed with an increase of elasticity, while in the main duct the intensity recirculation presents a non-monotone behaviour with the increase of elasticity. For both flow recirculations, intensities tend to vary strongly at low values of Deborah number and retardation ratios, inline with results presented before for the recirculation length variations. In the case of the vertical recirculation and for high values of Deborah number and retardation ratios, the vortex intensity is insensitive to variations of De .

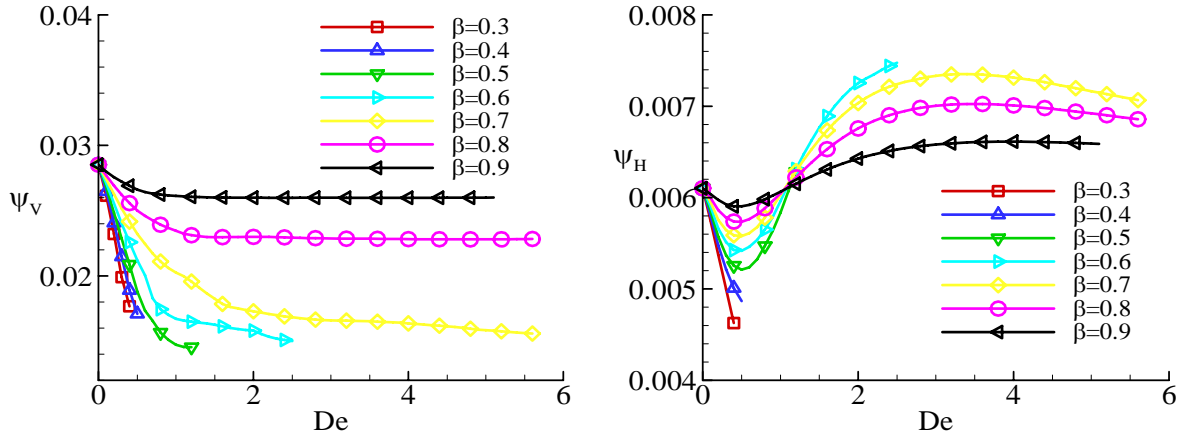


Figure 4- Variation of the vertical and horizontal vortex strength with De and β .

Figures 5 and 6 exhibit contour plots of velocity (U and V) and the shear stress (τ_{xy}) fields, in the bifurcation zone, for a constant retardation ratio and Deborah number. The results shown in these figures are in agreement with the literature in what refers to the existence of low velocity zones and shear stresses within the recirculation zones, thus promoting the adhesion of platelets, red cells and lipids, and the formation of atherosclerotic plaques. Simultaneously, in re-entrant corners very high shear stresses are registered, with positive and negative signs.

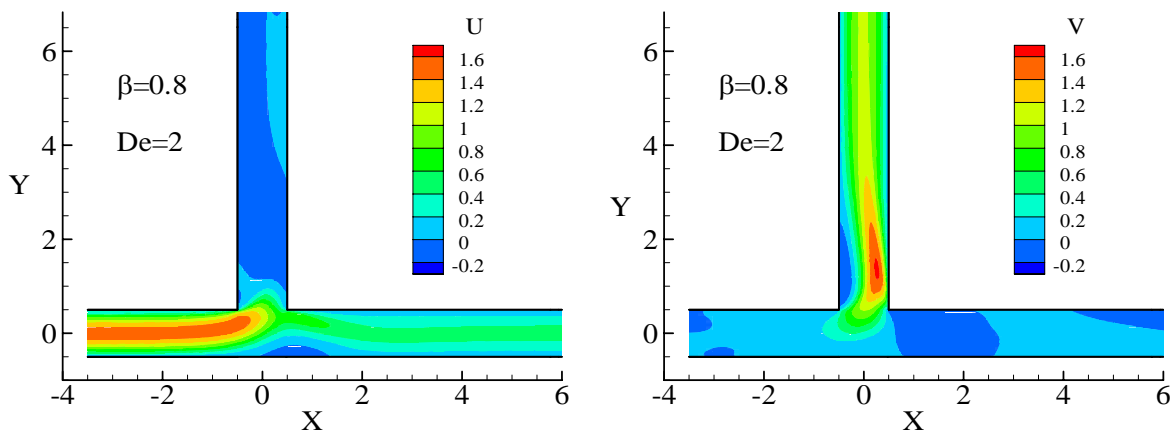


Figure 5- Variation of the velocity components fields for $\beta = 0.8$ and $De = 2$.

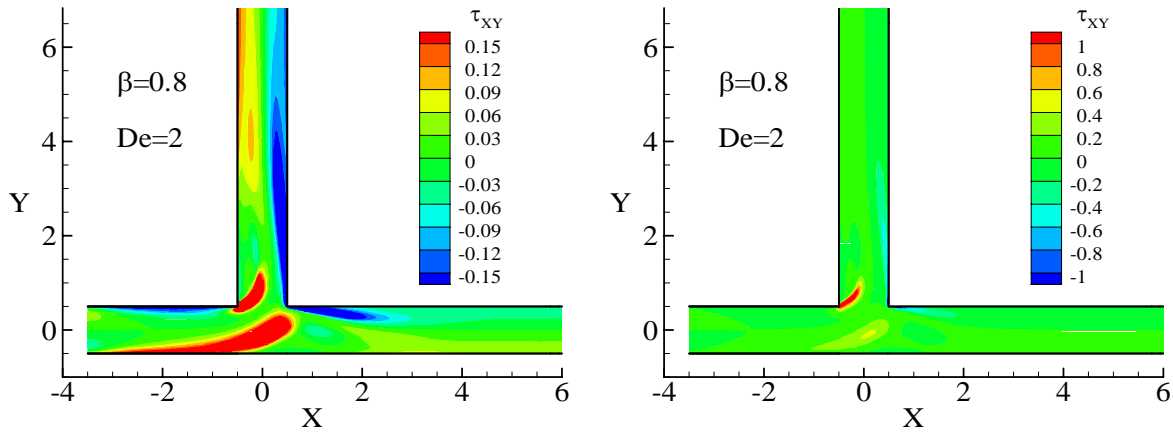


Figure 6- Variation of the shear stress field for $\beta = 0.8$ and $De = 2$.

The variation of the maximum and minimum shear stresses with the Deborah number and retardation ratio is illustrated in figure 7. The maximum shear stress occurs in the re-entrant corner at the proximal wall and increase with the increase of the elasticity for low values of Deborah, while for high values of Deborah number and β , a constant value of shear stress is obtained. In the re-entrant corner at the distal wall it is registered a minimum of shear stress with an increase in modulus as elasticity is raised at low values of Deborah, while for high values of Deborah the minimum shear stress value continues to increase in modulus with the increase of the polymer concentration, but decreasing with increase in Deborah number. For high values of Deborah and β a constant value of shear stress tends to be obtained as in the other re-entrant corner.

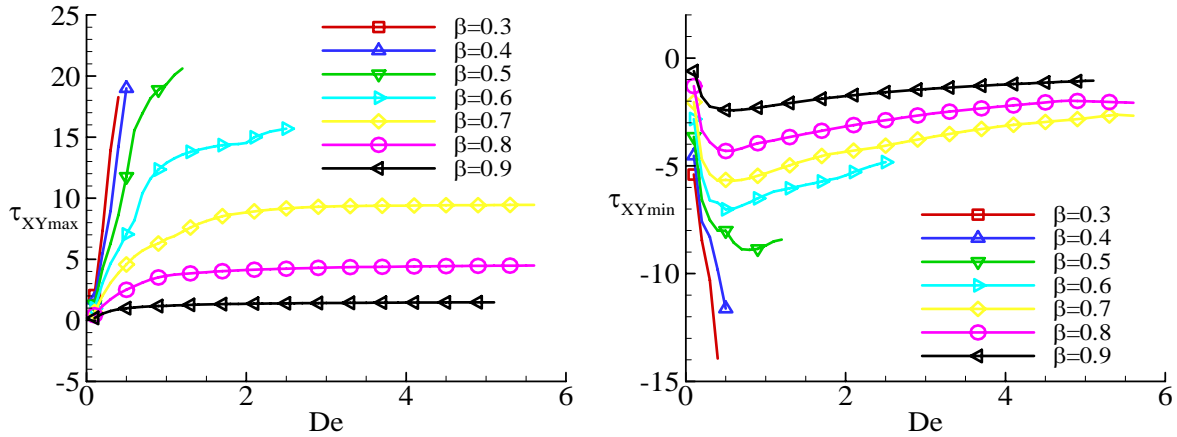


Figure 7- Variation of the maximum and minimum shear stresses with De and β .

In the set of figures shown, we have addressed the influence of elasticity through variation of Deborah number and retardation ratio. The results show a strong influence of elasticity upon the main flow characteristics, resulting in a reduction of recirculation length and intensity, and an increase of the shear stresses in a general way. So this influence cannot be ignored and must be included in two-phase flow simulations, in future works, in order to obtain more realistic predictions of flow behavior. Thus, in future works we intend to analyze the influence of the inclusion of particles in the main flow characteristics, and the use of viscoelastic fluids in the phase separation efficiency when a T-junction is applied as a phase

separator, using as comparison the results of Issa and Oliveira (1994) for a Newtonian two-phase flow.

Acknowledgements

H.M.M. Matos wishes to acknowledge the financial support provided by Fundação para a Ciência e Tecnologia (FCT) through the grant SFRH/BD/18062/2004 and both authors acknowledge the financial support provided by FCT and FEDER through project POCTI/EME/58657/2004.

REFERENCES

- Alves, M. A., Oliveira, P. J. & Pinho, F. T., 2003. A convergent and universally bounded interpolation scheme for the treatment of advection. *International Journal for Numerical Methods in Fluids*, vol. 41, n. 1, pp. 47-75.
- Anand, M. & Rajagopal K. R., 2004. A shear-thinning viscoelastic fluid model for describing the flow of blood. *International Journal of Cardiovascular Medicine and Science*, vol. 4, n. 2, pp. 59-68.
- Baker, G., Clark, W. W., Azzopardi, J. B., & Wilson, J.A., 2007. Controlling the phase separation of gas-liquid flows at horizontal T-junctions. *AIChE Journal*, vol. 53, pp. 1908-1915.
- Bird, R. B., Hassager, O., Armstrong, R. C., & Curtiss, C. F., 1987. *Dynamics of polymeric liquids: Kinetic theory*. John Wiley & Sons, Vol. II.
- Caro, C. G., Fitz-Gerald, J. M. & Schroter, R. C., 1971. Atheroma and arterial wall shear observation, Correlation and proposal of a shear dependent mass transfer mechanism for atherogenesis. *Proc. Roy. Soc London, Ser.B*, vol. 177, n. 1046, pp. 109-133.
- Crowe, C. T., Sommerfeld, M., & Tsuji, Y., 1998. *Multiphase Flow with Droplets and Particles*. CRC Press: Boca Raton.
- Chilcot, M. D. & Rallison, J. M., 1988. Creeping flow of dilute polymer solutions past cylinders and spheres. *Journal of Non-Newtonian Fluid Mechanics*. vol. 29, pp. 381-432.
- Dheur, J. & Crochet, M. J., 1989. Stratified flows of Newtonian and viscoelastic fluids. *Journal of Non-Newtonian Fluid Mechanics*, vol. 32, pp. 1-18.
- Ferziger, J. H. & Peric, M., 1996. *Computational methods for fluid dynamics*. Springer Verlag.
- Fry, D. L., 1969. Certain histological and chemical responses of the vascular interface to acutely induced mechanical stress in the aorta of the dog. *Circulation Research*, vol. 24, n. 1, pp. 93-108.

- Hatziaavramidis, D., Sun, B. & Gidaspow, D., 1997. Gas-liquid flow trough horizontal tees of branching and impacting type. *AIChE Journal*, vol.43, n. 7, pp.1675-1683.
- Issa R. I., & Oliveira, P. J., 1994. Numerical prediction of phase separation in two-phase flow through T-junctions. *Computers and Fluids*, vol. 23, n. 2, pp. 347-372.
- Joris, E., Zand, T. & Majno, G., 1982. Hydrodynamic injury of the endothelium in acute aortic stenosis. *American Journal of Pathology*, vol. 106, pp. 394-408.
- Jung J., Hassanein A. & Lyczkowski, 2006. Hemodynamic computation using multiphase flow dynamics in a right coronary artery. *Annals of Biomedical Engineering*, vol. 34, n.3, pp. 393-407.
- Ku, D. N., Giddens, D. P., Phillips, D. J. & Strandness, D. E., 1985. Hemodynamics of the normal human carotid bifurcation: in Vitro and in vivo studies. *Ultrasound in Medicine & Biology*, vol. 11, n. 1, pp. 13-26.
- Ku, D., 1997. Blood flow in arteries. *Annual Review of Fluid Mechanics*, vol. 29, pp. 399-434.
- Leuprecht, A. & Perktold, K., 2001. Computer simulation of non-Newtonian effects on blood flow in large arteries. *Computer Methods in Biomechanics and Biomedical Engineering*, vol. 4, n. 2, pp. 149-163.
- Liesch, D., Moravec, S., Rastogi, A. K. & Vlachos, N. S., 1982. Measurement and calculations of laminar flow in a ninety degree bifurcation. *Journal of Biomechanics*, vol. 15, pp. 473-485.
- Long, J. A., Ündar, A., Manning, K. B. & Deutsch, S., 2005. Viscoelasticity of pediatric blood and its implications for the testing of a pulsatile pediatric blood pump. *ASAIO Journal*, vol. 51, pp. 563-566.
- Margaris, P. D., 2007. T-junction separation modelling in gas-liquid two-phase flow. *Chemical Engineering and Processing*, vol. 47, pp. 150-158.
- Matos, H. M. M., Alves, M. A., & Oliveira, P. J., 2007a. Viscoelástico flow through a two-dimensional T-Junction. *CMNE/CILANCE-2007*, Porto, Portugal, Jun. 13-15, pg. 365. (in Portuguese).
- Matos, H. M. M., Alves, M. A., & Oliveira, P. J., 2007b. New formulation for stress calculation: Application to flow in a T-Junction with viscoelastic fluids. *The Society of Rheology 79th Annual Meeting*, Salt Lake City, USA, Oct. 7-11.
- Matos, H. M. M., Alves, M. A., & Oliveira, P. J., 2007c. Viscoelastic flow through a two-dimensional T-Junction: The study of elasticity variation. *Engenharias 2007 - Inovação e Desenvolvimento*, Covilhã, Portugal, Nov. 5-7. (in Portuguese).
- Miranda A. I. P., Oliveira P. J. & Pinho F. T., 2008. Steady and unsteady laminar flows of Newtonian and generalized Newtonian fluids in a planar T-junction. *International Journal for Numerical Methods in Fluids*, vol. 57, n. 3, pp. 295-328.

- Oliveira, P. J., 1992. *Computer modelling of multidimensional multiphase flow and application to T-junctions*. PhD thesis, Imperial College, University of London.
- Oliveira, P. J., Pinho, F. T. & Pinto, G. A., 1998. Numerical simulation of non-linear elastic flows with a general collocated finite-volume method. *Journal of Non-Newtonian Fluid Mechanics*, vol. 79, n. 1, pp. 1-43.
- Oliveira, P. J. & Pinho, F. T., 1999. Numerical procedure for the computation of fluid flow with arbitrary stress-strain relationships. *Numerical Heat Transfer, Part B*, vol. 35, n. 3, pp. 295-315.
- Oliveira, P. J. & Issa, R. I., 2003. Numerical aspects of an algorithm for the Eulerian simulation of two-phase flows. *International Journal for Numerical Methods in Fluids*, vol. 43, pp. 1177-1198.
- Owens, R. G., 2006. A new microstructure-based constitutive model for human blood. *Journal of Non-Newtonian Fluid Mechanics*, vol. 140, n.1-3, pp. 57-70, 2006.
- Patankar, S. V., 1980. *Numerical heat transfer and fluid flow*. Hemisphere.
- Rhie, C. M. & Chow, W. L., 1983. A numerical study of the turbulent flow past an airfoil with trailing edge separation. *AIAA Journal*, vol. 21, n. 11, pp. 1525-1533.
- Richardson, L. F., 1910. On the approximate arithmetical solution by finite differences of physical problems involving differential equations with an application to the stresses in a masonry dam. *Proc. Roy. Soc London Ser. A*, vol. 83, n. 563, pp. 335-336.
- Salzar, R. S., Thubrikar, M. J. & Eppink, R. T., 1995. Pressure-induced mechanical stress in the carotid artery bifurcation: a possible correlation to atherosclerosis. *Journal of Biomechanics*, vol. 28, n. 11, pp. 1133-1340.
- Shah, R. K. & London, A. L., 1978. *Laminar flow forced convection in ducts*. Academic Press, New York.
- Van Doormaal, J. P., & Raithby, G. D., 1984. Enhancements of the SIMPLE method for predicting incompressible fluid flows. *Numerical Heat Transfer, Part A*, vol. 7, n. 2, pp. 147-163.
- Wang, L.-Y., Wu, Y.X., Zheng, Z.-C., Guo, J. Zhang, J. & Tang, C., 2008. Oil-water two-phase flow inside T-junction. *Journal of Hydrodynamics*, vol. 20, n. 2, pp. 147-153.
- Zarins, C. K., Gieddens, D. P., Bharadaj, B. K., Sotturai, V. S., Mabon, R. F. & Glagov, S., 1983. Carotid bifurcation atherosclerosis: Quantitative correlation of plaque localization with flow velocity profiles and wall shear stress. *Circulation Research*, vol. 53, n. 4, pp. 502-514.